Cerium *d*-Block Element (Co, Ni) Bimetallic Oxides as Catalysts for the Methanation of CO₂: Effect of Pressure

Joaquim Miguel Badalo Branco [1,2,*], Ana Cristina Ferreira [1] and Joana Filipa Martinho [1]

1   Centro de Química Estrutural, Instituto Superior Técnico Universidade de Lisboa,
    Campus Tecnológico e Nuclear, Estrada Nacional 10, ao km 139.7, 2695-066 Bobadela, Portugal;
    acferreira@ctn.tecnico.ulisboa.pt (A.C.F.); joana.martinho@ctn.tecnico.ulisboa.pt (J.F.M.)
2   Departamento de Engenharia e Ciências Nucleares, Instituto Superior Técnico, Universidade de Lisboa,
    Campus Tecnológico e Nuclear, Estrada Nacional 10, ao km 139.7, 2695-066 Bobadela, Portugal
*   Correspondence: jbranco@ctn.tecnico.ulisboa.pt

Abstract: Nickel– and cobalt–cerium bimetallic oxides were used as catalysts for the methanation of CO_2 under pressure. The catalysts' activity increases with pressure and an increase of just 10 bar is enough to double the yield of methane and to significantly improve the selectivity. The best results were those obtained over nickel–cerium bimetallic oxides, but the effect of pressure was particularly relevant over cobalt–cerium bimetallic oxides, which yield to methane increases from almost zero at atmospheric pressure to 50–60% at 30 bar. Both catalyst types are remarkably competitive, especially those containing nickel, which were always more active than a commercial rhodium catalyst used as a reference ($5_{wt.\%}$ Rh/Al_2O_3) and tested under the same conditions. For the cobalt–cerium bimetallic oxides, the existence of a synergetic interaction between Co and CoO and the formation of cobalt carbides seems to play an important role in their catalytic behavior. Correlation between experimental reaction rates and simulated data confirms that the catalysts' behavior follows the *Langmuir–Hinshelwood–Hougen–Watson* kinetic model, but *Le Chatelier*'s principle is also important to understand the catalysts' behavior under pressure. A catalyst recycle study was also performed. The results obtained after five cycles using a nickel–cerium catalyst show insignificant variations in activity and selectivity, which are important for any type of practical application.

Keywords: carbon dioxide; methanation; cerium oxide; pressure; preparation method

1. Introduction

The control of CO_2 emissions is an important matter that can be achieved by reducing the amount of CO_2 discharged into the atmosphere; storing CO_2; or employing CO_2 as feedstock, aiming to produce value-added products such as chemicals and fuels [1]. This last path is the most promising.

In fact, CO_2 is a cheap and attractive carbon source that can be used to produce a variety of raw materials, e.g., methane and methanol, making it one of the most attractive options to reduce the greenhouse effect. Additionally, methane itself can be used to produce many other chemicals and is an important energy carrier that can be used in many sectors, such as the power, household, and transportation industries.

Among relevant industrial applications, the methanation of CO_2 is at the core of the Power-to-Gas (PtG) technology for renewable energy storage [2]. The natural gas network is already well established and synthetic renewable CH_4 produced via PtG can be added to the existing grid, not only to compensate for any fluctuations, but, in the future, to fully replace natural gas from fossil sources [2,3]. The hydrogen needed for the methanation of CO_2 can be obtained from renewable resources, such as biomass gasification, wind power, or solar water-splitting [4–6].

Nickel-based catalysts have been at the center of many CO_2 methanation studies, namely due to their good activity and cheaper costs [7,8]. Moreover, Ni and other metals

such Co [4,9,10] continue to be studied as alternatives to those based on noble metals, e.g., Ru [11], Rh [12], or Pd [13], that are more active but also much more expensive. However, traditional Ni catalysts suffer from deactivation by sintering, coke deposition, and the formation of volatile nickel carbonyls at high temperatures [14]. The best way to overcome such problems is to decrease the temperature or to increase the reaction pressure so that it favors the formation of CH_4 and prevents the deposition of coke [15,16]. The advantages of pressure conditions, in terms of reaction kinetics and thermodynamics, are known [17,18], and the effects of pressure conditions on syngas production have been studied over the last 90 years [19,20]. To our knowledge, most of the studies so far published focus on the hydrogenation of CO_2 at elevated pressure points for the production of syngas or methanol, the latter at pressures ranging from 40 to 100 bar [21–23]. The effect of pressure on the methanation of CO_2 is an issue that continues to be largely unexplored, especially in the case of nickel-based catalysts that already show very good activity at atmospheric pressure [16]. However, a few recent studies were performed in order to increase the catalytic activity to methane of less active metals, e.g., Fe and Co, at relatively low pressures (5–30 bar) and the results are indeed very promising [24–30].

Herein, we describe the effect of low pressures ($\leq$30 bar) on the catalytic behavior of nanostructured nickel– and cobalt–cerium bimetallic oxide catalysts for the methanation of CO_2 at 300 °C. This work complements that previously carried out by our group at atmospheric pressure [31]. In fact, the results over nickel–cerium bimetallic oxides were excellent at atmospheric pressure, but the results obtained over cobalt–cerium bimetallic oxides presented low or moderate activity. Therefore, we thought that under pressure the catalytic activity of such systems could be improved, which did happen. The results were compared to those obtained under the same conditions over a commercial catalyst of rhodium supported on alumina (5$_{wt.\%}$ Rh) as a reference. Additional tests were also carried out over reused samples in order to strengthen the viability of nickel– and cobalt–cerium bimetallic oxides as catalysts for the methanation of CO_2 [31].

2. Results and Discussion

2.1. Characterization of Catalysts before Catalytic Reaction

All fresh catalysts were textural and morphologically characterized by X-ray diffraction, scanning electron microscopy–energy dispersive spectroscopy, and the nitrogen adsorption−desorption Brunauer–Emmett–Teller (BET) method. Their reducibility/redox properties were evaluated by temperature-programmed reduction under hydrogen (H_2-TPR), whereas their acid-base properties were evaluated using the dehydrogenation/dehydration of 2-propanol as a reaction model. The characterization was described in our previous publication where these catalysts were tested for CO_2 methanation at atmospheric pressure [31].

The morphology observed for the catalysts obtained by sol−gel methodologies (Epoxide addition and *Pechini*) can be described as a spongy structure typical of an aerogel that comprises a network of sphere-shaped nanoparticles containing the metal elements (20–50 nm in diameter). The catalysts prepared by Electrospinning present a nanofiber structure with external diameters covering a wide range of 250−500 nm. Regarding the preparation method, the cubic phase of CeO_2 was the main phase confirm by XRD along with the cubic phases of NiO or Co_3O_4. After pre-reduction treatment, the phases observed were the metallic phase of the d-block element (Ni or Co) and CeO_2.

The preparation method influences BET surface areas, redox, and acid-base properties of cerium-based catalysts (Table 1). The BET surface areas increase following this order: Epoxide addition method ($\approx$37 m^2/g) < *Pechini* method ($\approx$46 m^2/g) < Electrospinning technique ($\approx$66 m^2/g). Considering the reducibility/redox properties, the interaction of NiO or Co_3O_4 species with CeO_2 presented different degrees of interaction, which are method dependent and increase in the following order (increase of Tm values): Epoxide $\leq$ Electrospinning < *Pechini*. It was also possible to confirm that all catalysts are basic, and

that the population of basic sites is higher on nickel samples than on cobalt samples. It is also higher on the nanofibers compared to nanoparticles.

Table 1. Characterization of nickel– and cobalt−cerium bimetallic oxides by BET, H_2-TPR, SEM/EDS, and dehydrogenation/dehydration of 2-propanol (acidity/basicity).

Preparation Method	Surface Area [a]		H_2-TPR		Basicity	EDS (Atomic Ratio
	m^2/g	m^2/gNi or Co	T_m (°C)	mol_{H2}/mol_{cat} [b]	$\upsilon A/\upsilon P$ [c]	Ni or Co/Ce) [d]
3NiO.CeO$_2$						
Epoxide addition	42.5	0.57	330	3.0	36.6	2.8
Pechini	46.8	3.25	179, 374, 733	2.9	146.4	2.7
Electrospinning	73.6	1.17	336, 697	3.0	252.9	2.9
Co$_3$O$_4$.CeO$_2$						
Epoxide addition	29.5	0.84	341, 382, 655	3.9	244.0	2.8
Pechini	44.2	0.78	286, 434, 714	3.8	370.0	2.8
Electrospinning	58.2	1.15	300, 356, 683	4.1	717.0	3.0

([a]) BET method (P/Po = 0.3); metallic areas measured by the N_2O method [32]; ([b]) and ([d]) Theoretical values 3, error ±0.1; ([c]) Between the ratio of the reaction rates of formation of acetone (A) and propene (P).

2.2. Methanation of CO$_2$ under Pressure

Figures 1 and 2 show the effect of pressure on the yield and selectivity to methane over fresh nickel– and cobalt–cerium bimetallic oxides, respectively. Clearly, the pressure enhances the catalysts' yield and selectivity to CH_4. The best results were those obtained nickel-based catalysts followed by the rhodium catalyst supported on alumina and cobalt-based catalysts, ($\approx$70% vs. $\approx$ 50% vs. $\approx$10% at 10 bar, respectively). The selectivity to methane was always very high over nickel and rhodium catalysts ($\geq$97%, at pressures $\geq$10 bar), but in the case of the cobalt catalyst obtained by the Electrospinning technique, it increased significantly with pressure, e.g., 85% vs. 21% at 30 and 1 bar, respectively. However, the values were always lower than those measured over nickel and rhodium catalysts.
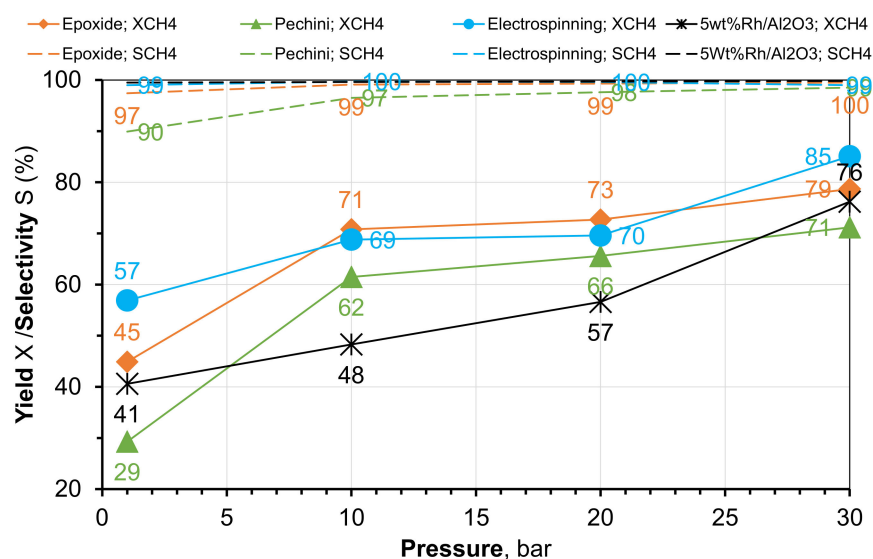
Figure 1. Methanation of CO$_2$ over fresh nickel–cerium bimetallic oxides at 300 °C: pressure and method effect on the yield to CH_4.
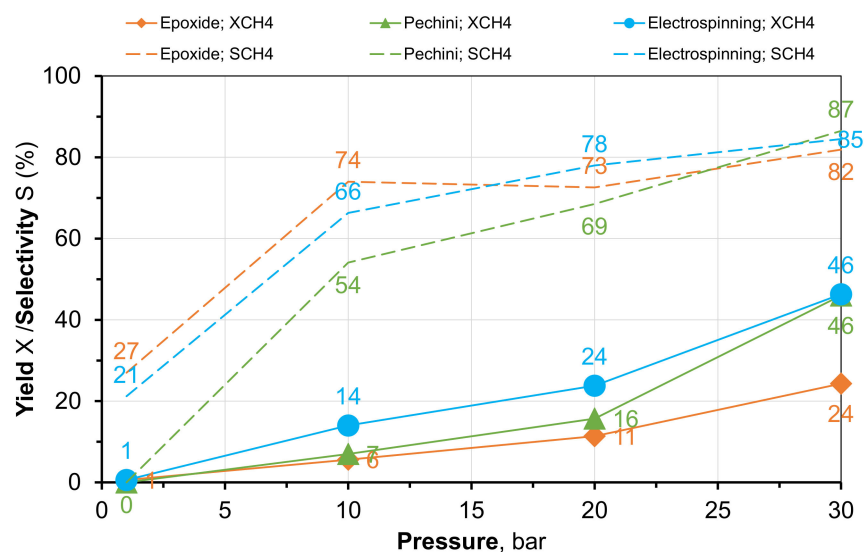
Figure 2. Methanation of CO_2 over fresh cobalt–cerium bimetallic oxides at 300 °C: pressure and method effect on the yield to CH_4.

Catalysts' performance seems also to depend on the catalysts' preparation method. The best catalytic results were those obtained over samples prepared by the Electrospinning technique, which is more obvious for the cobalt catalysts (Figure 2). In the case of the nickel catalyst, very good results were also obtained over those prepared by the Epoxide addition method; the differences between this method and the Electrospinning technique are not significant, except at atmospheric pressure (1 bar). Regardless of the preparation method, all nickel catalysts are, in general, more active than the rhodium catalyst. While for cobalt catalysts the activity increases linearly with the pressure (it seems to double each time that the pressure doubles), for nickel catalysts the activity increases significantly from 1 to 10 bar, but the effect of pressure is not significant at higher pressures (it reaches a plateau). The major selectivity improvement occurs also at 10 bar, which is significant since low-pressure experimental facilities can be easily implemented. This is an advantage for any future practical applications.

The behavior of cobalt catalysts merits an additional remark since CH_4 yields and selectivities obtained at 30 bar (40% and 80%, respectively) over the catalysts prepared by the Electrospinning technique and the *Pechini* method are important and to our knowledge not often reported in the literature [33]. Moreover, recent studies have shown that the possibility of a synergetic reduction–oxidation cycle, ascribed to the reduction of CoO and the oxidation of metallic Co, seems to be the key factor to enhance cobalt-based catalysts' limited activity for the methanation of CO_2 [34].

Taking that into consideration, we have studied the effect of pressure over reused nickel– and cobalt–cerium bimetallic oxides recovered from our previous CO_2 methanation studies at atmospheric pressure in the same temperature range (250–500 °C). Moreover, in the case of our cobalt catalysts, the presence of both CoO and metallic Co phases after the catalytic studies could be confirmed by powder XRD analysis [31]. The results obtained show a catalytic behavior that is very similar over fresh and reused nickel–cerium catalysts, with minor variations in activity and selectivity to methane, mostly over the catalysts obtained by the *Pechini* and Epoxide addition methods (Figures S1–S4). Instead, the activity and selectivity toward methane over cobalt–cerium catalysts are surprisingly better over the reused samples of those obtained by the *Pechini* method and Electrospinning technique. The activity is comparable to that obtained over the rhodium catalyst without any pretreatment under hydrogen at pressures $\geq$ 10 bar and remarkably better at 30 bar (Figures 3 and 4). At such pressure, the activity is significantly higher, almost double the activity of the rhodium catalyst (71 vs. 39%) and is similar to that obtained over the

nickel–cerium catalysts prepared by the Epoxide addition and *Pechini* and methods (74%). This is a very good result and to our knowledge rarely reported in the literature.
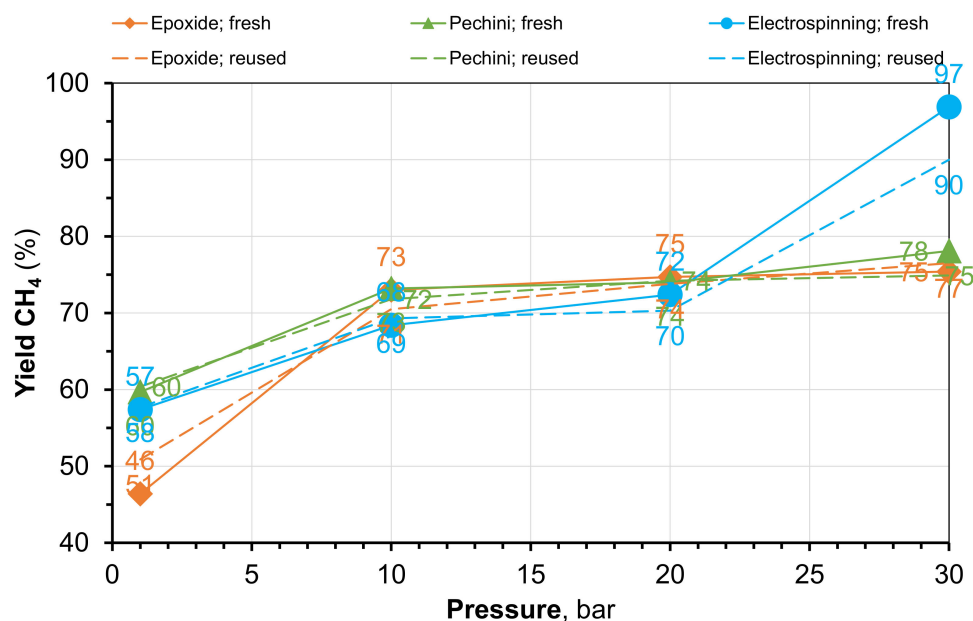
Figure 3. Methanation of CO_2 over reused nickel–cerium bimetallic oxides at 300 °C without pretreatment under hydrogen: effect of preparation method on yield to CH_4.
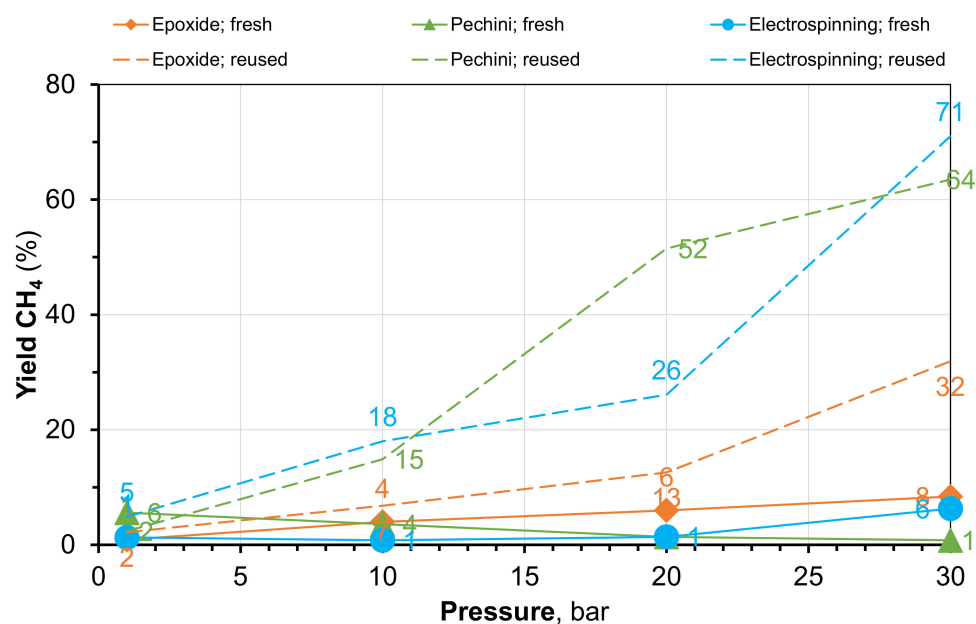
Figure 4. Methanation of CO_2 over reused cobalt–cerium bimetallic oxides at 300 °C without pretreatment under hydrogen: effect of preparation method on yield to CH_4.

In addition, any comparison between our results and those reported by other authors is difficult, if not impossible, due to differing experimental conditions, namely in terms of GHSV and temperature (Table 2). That is why we decided to test, in the same experimental conditions as this study, a commercial rhodium catalyst supported on alumina (5$_{wt.\%}$ Rh/Al$_2$O$_3$) using the results obtained for comparison. It can be said that nickel–cerium catalysts are clearly competitive when compared to the rhodium catalyst supported on alumina. Cobalt–cerium catalysts also present good activity, namely the reused catalysts

obtained by the Electrospinning technique. They have an activity comparable to those found in the literature, although under very different conditions. This result reinforces the relevance of low pressure conditions as a way to enhance catalysts' activity and the potential of cobalt-based catalysts for the methanation of CO_2.

Table 2. Comparison of catalysts' activity.

Catalyst	Conditions (T °C, P Bar, GHSV mL/g.h)	Yield CH_4 (%) [a]	Sel CH_4 (%) [a]	Sel CO (%) [a]	Ref.
$3NiO.CeO_2$ Epoxide	300, 30, 15,000	78.7 (76.5)	99.5 (99.8)	0.5 (0.2)	This work
$3NiO.CeO_2$ *Pechini*	300, 30, 15,000	71.2 (74.9)	98.5 (99.8)	0.9 (0.2)	This work
$3NiO.CeO_2$ Electrospinning	300, 30, 15,000	85.1 (90.0)	99 (98.4)	1 (1.6)	This work
$Co_3O_4.CeO_2$ Epoxide	300, 30, 15,000	24.3 (31.9)	81.9 (85.9)	7.7 (14.1)	This work
$Co_3O_4.CeO_2$ *Pechini*	300, 30, 15,000	46.0 (63.5)	86.5 (96.3)	5.6 83.7)	This work
$Co_3O_4.CeO_2$ Electrospinning	300, 30, 15,000	46.3 (71.0)	84.5 (97.4)	5.3 (2.6)	This work
$5_{wt.\%}$ Rh/Al_2O_3	300, 30, 15,000	86.2	99.8	0.2	This work
$Co/Ce_{0.8}Zr_{0.2}O_2$	320, 15, 15,000	80.4	99	1	[30]
Co/ZrO_2	400, 30, 7200	84.2	99	1	[26]
Co/ZrO_2	400, 30, 3600	92.4	99.9	0.1	[29]
Co nanorods	300, 10, 18,000	78.4	98	2	[28]
$Zr-Co_3O_4$	200, 5, 18,000	58.2	100	0	[27]

([a]) The values obtained with reused catalysts are between parentheses.

A catalyst recycle study using the nickel–cerium catalyst synthetized by the *Pechini* method (Figure 5) was also undertaken. The results obtained after five cycles show that such a catalyst is stable without significant variation in activity and selectivity (loss of ≈10% in yield; loss in selectivity inferior to 1%), which is important for any type of practical application.
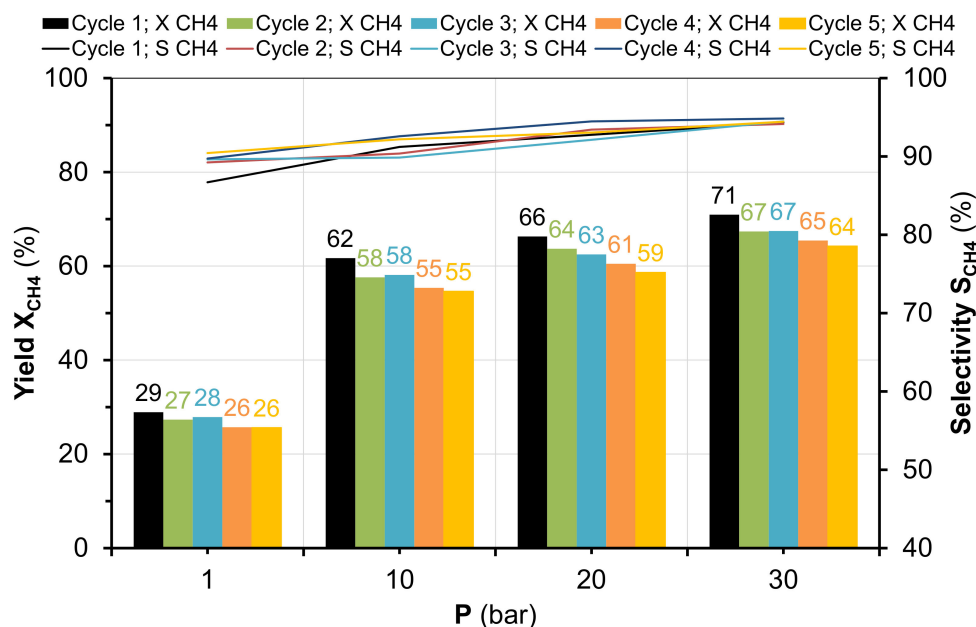
Figure 5. Recycle study performed over the nickel–cerium bimetallic oxide catalyst at 300 °C pretreatment under hydrogen: cycle 1 black; cycle 2 green; cycle 3 blue; cycle 4 orange.

2.3. Characterization of Catalysts after Catalytic Reaction

To explain such results, we must consider the catalysts' evolution during the reaction and the effect of the pre-reduction treatment on their chemical composition and structure. The literature shows that pre-treatment under hydrogen enhances catalysts' activity for the methanation of CO_2, which is explained by the formation and densification of the metallic active sites at the surface [35].

The analysis of nickel–cerium catalysts by powder XRD confirms that before treatment under hydrogen, the only oxides phases detected were those of NiO and CeO_2. After pre-treatment under hydrogen and reaction under pressure (fresh or reused), only the patterns of CeO_2 and Ni could be observed (Figure 6 and Figure S5, respectively). Such results explain the weak catalytic behavior variations observed over such catalysts, regardless of the preparation method or the pre-treatment. Indeed, the formation of the main active species (metallic Ni) can easily occur at 300 °C (reaction temperature used in this study) under a reductive atmosphere [36].
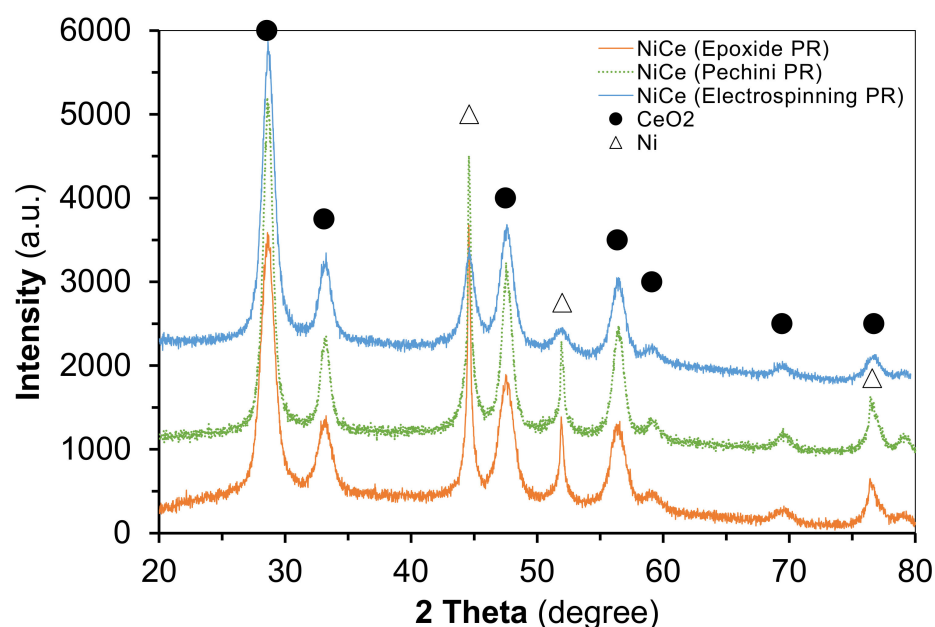
Figure 6. Nickel–cerium bimetallic oxides prepared by different methods: XRD analysis (powder) after tests under pressure over fresh samples.

In the case of the cobalt-based catalysts, CeO_2 along with metallic cobalt were the only species detected after reaction over fresh pre-reduced samples (Figure 7a), whereas over reused catalysts without pre-treatment under hydrogen, the oxide phases detected were metallic Co, CoO, and CeO_2 (Figure 7b). The fresh cobalt catalysts were pre-reduced at 450 °C. The need for such high temperature is important since under a reductive atmosphere, lower temperatures are not enough to fully reduce the cobalt oxide phase (Co_3O_4) to Co [37], e.g., at 300 °C, explaining the presence of CoO on the reused catalysts with no pre-treatment. Therefore, considering that the best results were those obtained over reused samples, the synergetic co-existence/cooperation between metallic cobalt and CoO, already reported by other authors, seems to be a key factor to improving the methanation of CO_2 over cobalt-based catalysts [34].

(**a**)

(**b**)
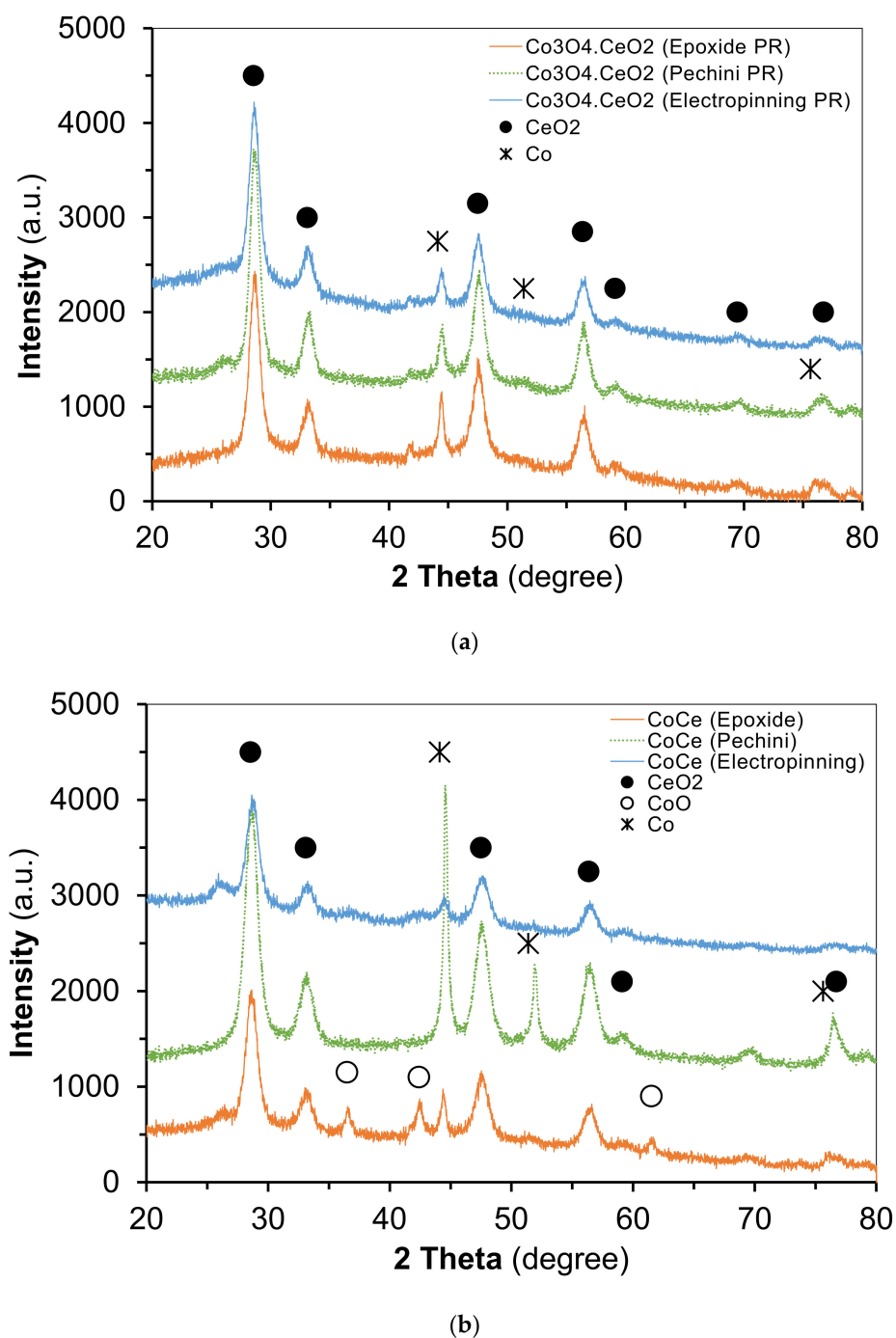
Figure 7. Cobalt–cerium bimetallic oxides prepared by different methods: XRD analysis (powder) after tests under pressure over fresh and reused catalysts, (**a**) and (**b**), respectively.

Further characterization of the catalysts was accomplished by temperature-programmed oxidation (O_2-TPO) studies that allow not only the oxidation and quantification of carbon, but also the oxidation and quantification of any fraction of metallic active species (Ni and Co) present on the catalysts after a reaction. The profiles obtained are easily distinguishable and understandable because the oxidation of carbon corresponds to a negative peak, whereas the peak related to the oxidation of any metallic fraction of Ni or Co is positive (Figure 8 and Figure S6).

(**a**)

(**b**)
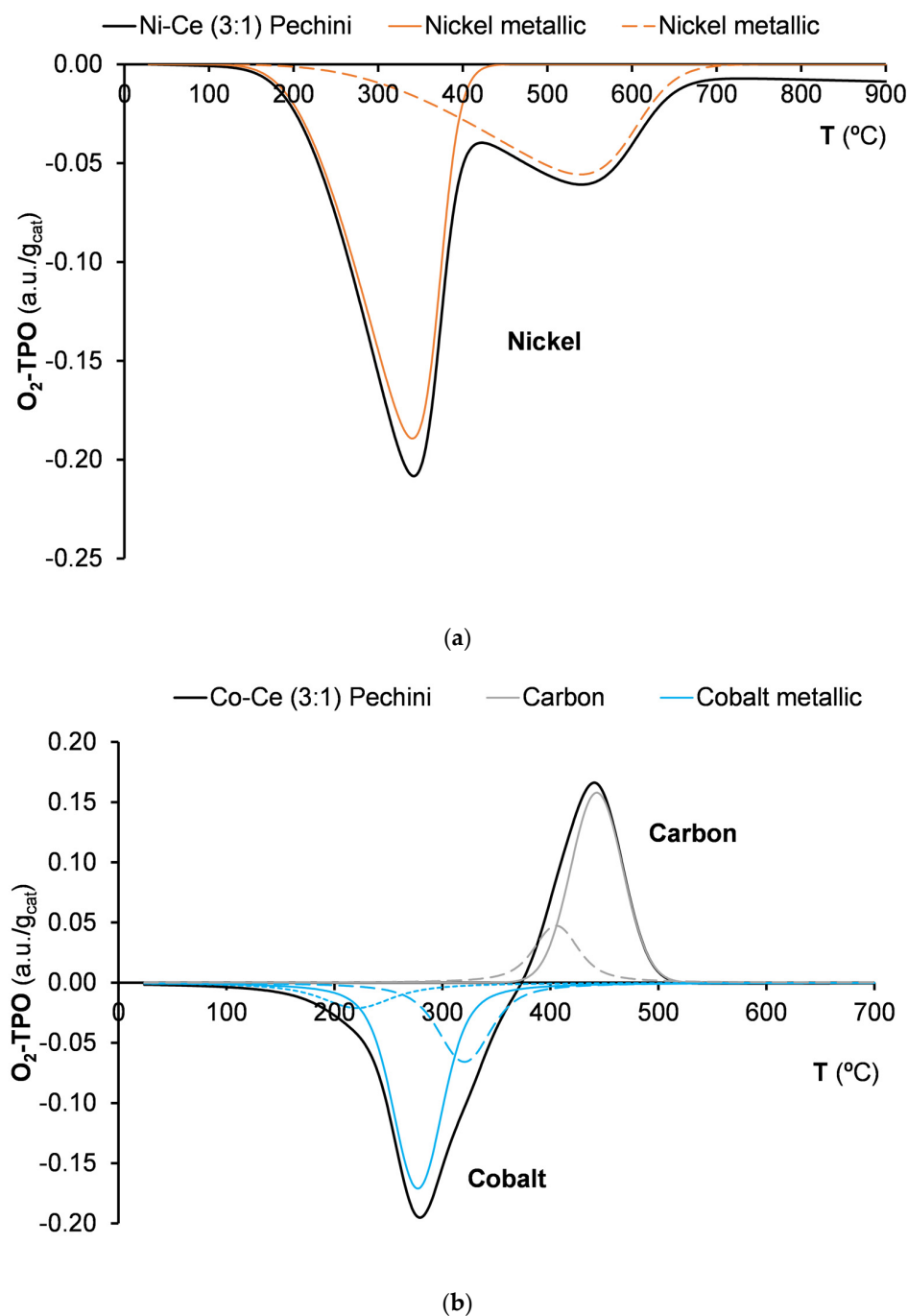
Figure 8. O_2-TPO profiles obtained after reaction for (**a**) nickel–cerium and (**b**) cobalt–cerium bimetallic oxides catalysts pre-treated under hydrogen and prepared by the *Pechini* method.

The O_2-TPO profiles show that the amount of carbon is below the detection limit over the nickel-based catalysts and over the $5_{wt.\%}$ Rh/Al_2O_3 (<0.01 wt.%; 0.0001 g/g_{cat}) (Figure 8a and Figure S6a,c). It is an unusual result but not a surprise taking into account that pressure prevents coke deposition [15,16]. On the other hand, over cobalt-based catalysts, high and measurable amounts of carbon were detected (Figure 8b and Figure S6b,d), which seems to be associated to the preparation method: higher over the nanofibers (Electrospinning) and lower over the nanoparticles (Epoxide, *Pechini*).

Moreover, the quantification of the results shows that the amount of metallic fraction present on the catalysts after a reaction seems also to be associated with the preparation method: higher over the nanofibers (Electrospinning) and lower over the nanoparticles

(Epoxide, *Pechini*). The catalysts' activity follows the amount of such metallic nickel, which is also true for both metals, except for the cobalt sample prepared by the Electrospinning technique (fibers) (Figure 9). We have also found that the activity of the cobalt samples seems directly proportional to the carbon content. The most striking behavior is that of the samples prepared by the Electrospinning technique, the most active are those with the lowest content of cobalt and the highest content of carbon.
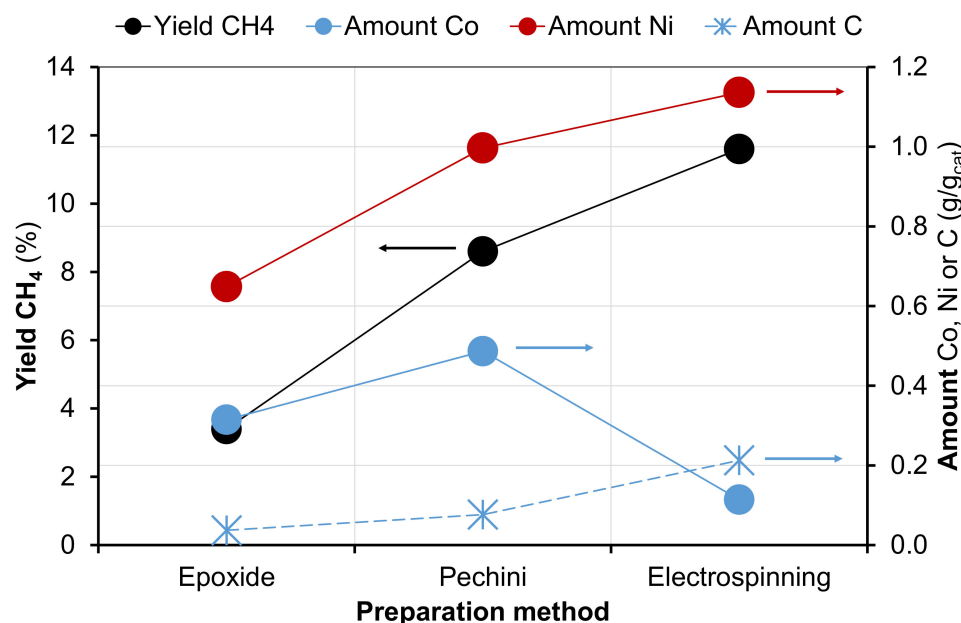
Figure 9. Correlation between catalytic activity at 10 bar/300 °C and amounts of Co, Ni and C on samples prepared by different methods (Epoxide addition and *Pechini* methods and Electrospinning technique).

To explain such a result, we must consider that cobalt–carbon nanostructures have recently attracted attention due to their unique tunable properties and interesting applications, e.g., fuel cell, catalysts support, growing exponentially every year [38–43]. Among them, cobalt carbides, e.g., Co_2C and Co_3C, are well known. Their preparation methods include, among others, Electrospinning and subsequent carbonization [44].

Moreover, to confirm the extent of carbonization, H_2-TPR (temperature-programmed reduction under hydrogen) studies are normally performed; it is known that the carbide phase shows a rapid transition to cobalt metal in a H_2 environment at a temperature of ~200 °C [40]. Our H_2-TPR results are consistent with this information (Figure 10). Clearly, the samples prepared by the Electrospinning technique show a first reduction peak that can be attributed to the carbides at ~200 °C and a second reduction attributed to the reduction of CoO at ~390 °C, in agreement with the XRD data obtained after the reaction where the diffraction patterns of Co and CoO could be identified. The carbide phases can be also characterized by XRD but, unfortunately, the poor crystallinity of our samples does not allow for any conclusion. However, the formation of cobalt carbide species that are catalytically active for the methanation of CO_2 seems like a strong possibility to explain the unusual evolution of the activity with the carbon content, but further work is needed in order to confirm this hypothesis.
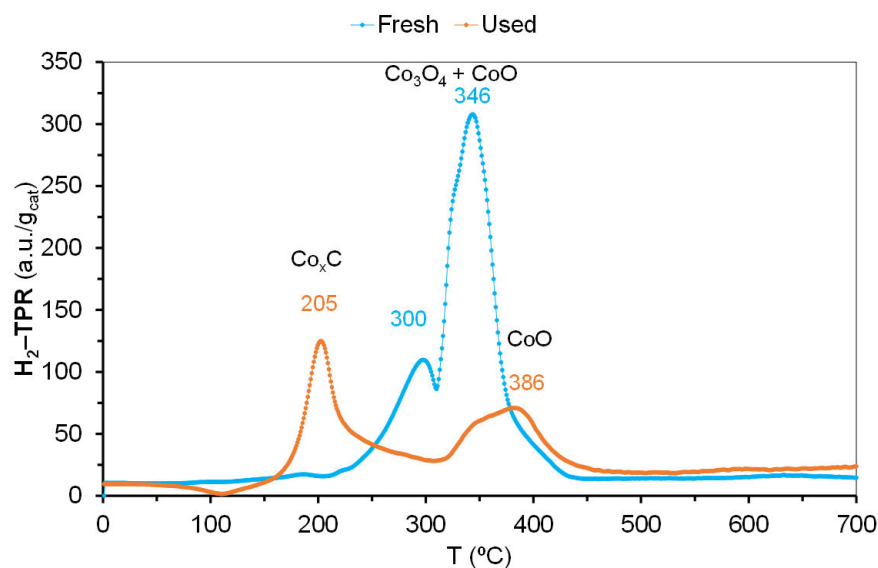
Figure 10. Comparison of H_2-TPR obtained before and after reaction for cobalt–cerium bimetallic oxides catalysts pre-treated under hydrogen obtained by the Electrospinning technique.

2.4. Kinetic Considerations

CO_2 methanation is a reversible and strongly exothermic reaction. It is thermo-dynamically favorable and is also a volume-reducing reaction ($CO_2 + 4H_2 \rightarrow CH_4 + 2H_2O$, $\Delta H^0_{298} = -164.9$ kJ/mol). However, the methanation of CO_2 is difficult to achieve due to the kinetic barriers related to the eight-electron-reduction process and the high temperatures typically needed (>300 °C) that also favor the undesired endothermic reverse water–gas shift (RWGS, $CO_2 + H_2 \rightarrow CO + H_2O$, $\Delta H^0_{298} = +41.3$ kJ/mol) reaction.

Two reaction paths have been proposed for the reduction of CO_2 to CH_4: the first involving the direct hydrogenation of CO_2 without passing through an intermediate [45,46] and the second involving the formation of an intermediate, carbon monoxide (CO). Nowadays, the most agreed-upon reaction mechanism seems to indicate that the reaction goes through the formation of CO and formates (via carbonate species) as reaction intermediates, with the transformation of CO_2 into CO being the limiting step [47,48]. The number of CO_2 methanation studies under pressure are still scarce and, to our knowledge, limited to a few cobalt- and nickel-based catalysts [16,28,49–51]. High pressures and low temperatures favor the reaction, e.g., at 30 bar and 300 °C, the influence of the RWGS is only important at temperatures higher than 450 °C [49]. Therefore, in order to understand the effect of pressure on our catalysts' behavior, kinetic investigations were undertaken and carried out at atmospheric pressure and at 30 bar in the temperature range 200–350 °C, where the methanation reaction is practically irreversible [52].

The only products detected were CH_4 and CO and the relation between reaction rates and temperature could be linearized (*Arrhenius* equation, constant composition of the reaction mixture), which indicates an exponential relation of the specific reaction rate constant, *k*, to the reagent concentrations (Figure 11, Equation (1)). Therefore, the kinetic equations can be described by rational power laws that correlate the reaction rate to the concentration of both reactants, in the absence of inhibition by the products, e.g., Equation (2).

$$k = A\, e^{-\frac{Ea}{RT}} \tag{1}$$

(where, E_a = energy of activation (kJ/mol), A = frequency factor, R = universal gas constant J/(mol K), and T = absolute temperature, K).

$$r_{CH_4} = k P_{H_2}{}^x P_{CO_2}{}^y \tag{2}$$

(where, r_{CH_4} = rate of formation of methane (mL per gram of catalyst per hour), k = specific reaction rate constant, P_{CO_2} and P_{H_2} = partial pressure of hydrogen and carbon dioxide (bar), x *and* y = order of reaction parameters for hydrogen and carbon dioxide, respectively).
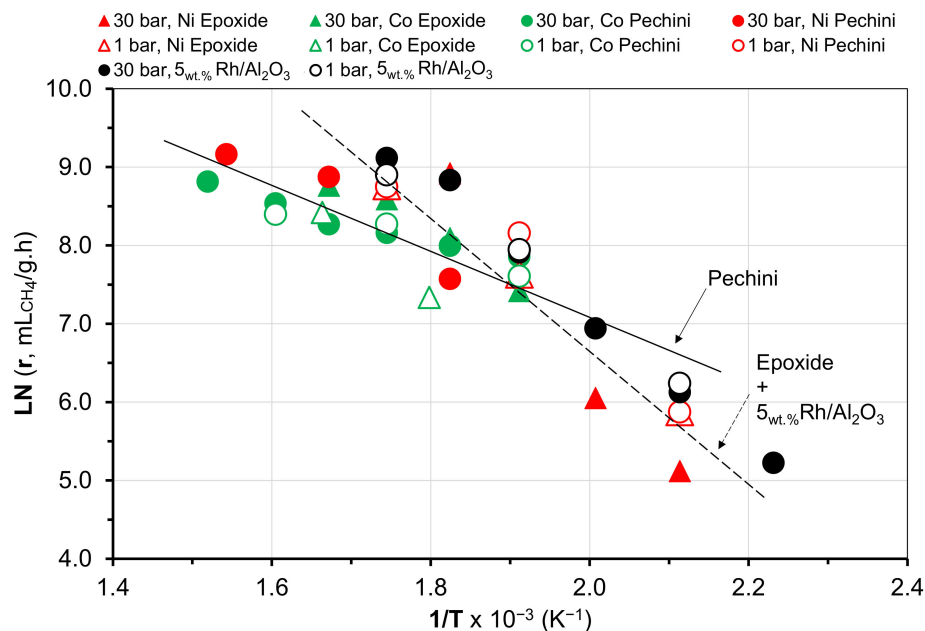
Figure 11. Relationship between reaction rates to temperature linearized in coordinates of the *Arrhenius* equation obtained for the catalysts prepared by the Epoxide addition and *Pechini* method and for the commercial rhodium catalysts ($5_{wt.\%}$ Rh/Al$_2$O$_3$) used as reference.

Moreover, concerning methanation reactions based on adiabatic reactors, the three most-used kinetic approach models are those based on a simple linear power law (Equation (2)), on the *Langmuir–Hinshelwood–Hougen–Watson* model [50] (Equation (3)), or on the *Chiang* and *Hopper* power-law-type equations [51] (Equations (4) and (5)). In this study, all three were used in order to simulate the catalysts' behavior and to correlate experimental with calculated data.

$$r_{CH_4} = \frac{\left(kP_{H_2}^{\frac{1}{3}} P_{CO_2}^{0.5}\right)}{\left(1 + k_1 P_{H_2}^{0.5} + k_2 P_{CO_2}^{\frac{1}{3}} + k_2 P_{CO_2}^{\frac{2}{3}} + k_3 P_{H_2O}\right)^2} \tag{3}$$

$$r_{CH_4} = \frac{\left(kP_{H_2}^4 P_{CO_2}\right)}{\left(1 + k_1 P_{H_2}^4 + k_2 P_{CO_2}\right)} \tag{4}$$

$$r_{CH_4} = \frac{\left(kP_{H_2}^4 P_{CO_2}\right)}{\left(1 + k_1 P_{H_2} + k_2 P_{CO_2}\right)^5} \tag{5}$$

The results obtained show clearly that the *Langmuir–Hinshelwood–Hougen–Watson* model (Equation (3)) and a simple power law with an H$_2$ order of reaction of 4 (Equation (2), $x = 4$ and $y = 1$, $r_{CH_4} = kP_{H_2}^4 P_{CO_2}^1$) can be noted as a hypothesis for all catalysts. However, the experimental data obtained under pressure for the nickel– and cobalt–cerium catalysts also shows also a good correlation with a *Chiang* and *Hopper*-type kinetic equation (Figure 12), as shown in Equations (4) and (5). For nickel catalysts, this agrees with the results published thus far, and for cobalt catalysts, this is being reported for the first time. In the case of the cobalt-based catalysts, a good correlation could be also obtained using

Equation (2) with an order of 0.25 for H_2 and 1 for CO_2, $r_{CH_4} = kP_{H_2}^{0.25} P_{CO_2}^{1}$, but the best fit was obtained using Equation (4), at least until pressures of 20 bar. Therefore, the specific reaction rates for the consumption of H_2 and CO_2 increase with the pressure, linearly in the case of the cobalt-based catalysts and following a more complex power law for nickel–cerium and rhodium catalysts.
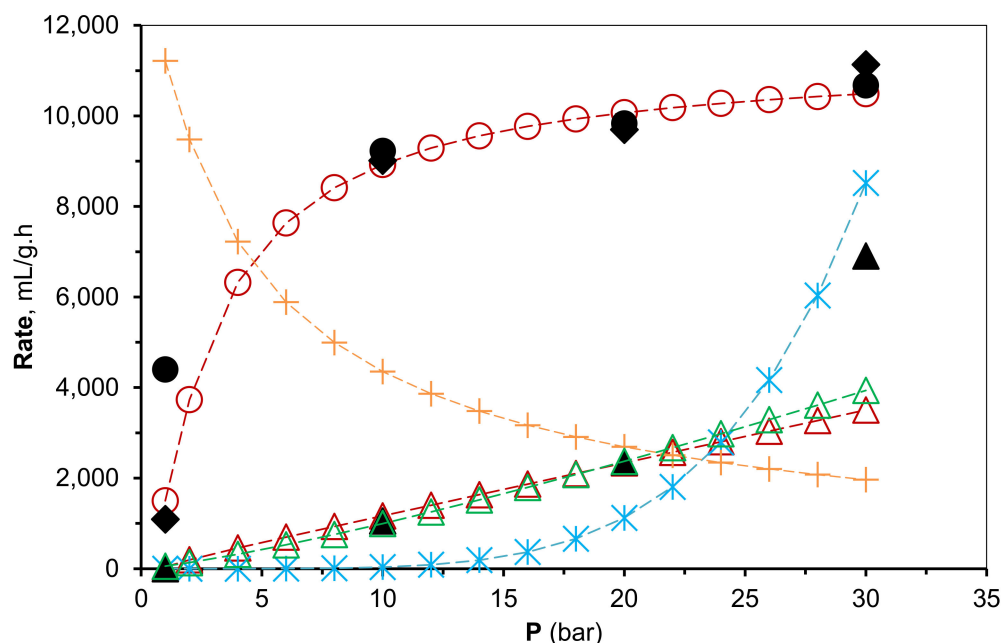
Figure 12. Correlation between experimental reaction rates obtained at 300 °C and 30 bar over nickel– and cobalt–cerium bimetallic oxides prepared by the *Pechini* method (filled black circle and filled black triangle, respectively) and simulated data (*Langmuir–Hinshelwood–Hougen–Watson* model power law: red circle, Equation (3); *Chiang* and *Hopper* power laws: red triangle, Equation (4) and orange cross, Equation (5); linear power laws, blue asterisk, Equation (2) *x* = 4, *y* = 1 and green triangle, Equation (2), *x* = 0.25, *y* = 1). Filled black lozenges correspond to the experimental data obtained over the reference catalyst ($5_{wt.\%}$ Rh/Al_2O_3).

Finally, under the premise of reactant concentration excess, which is definitely the case of the reactions under pressure, $P_{H_2}^{x} P_{CO_2}^{y}$ can be regarded as a constant (C) and Equation (2) can be rewritten as: $r_{CH_4} = kC$ or if substitute into Equation (1), $\ln r_{CH_4} = \ln(AC) - \frac{E_a}{RT}$. Therefore, the E_a values can be calculated from the $(\ln r_{CH_4})$ vs. $\left(\frac{1}{T}\right)$ plot (Figure 11 and Figure S7) and the results obtained were compiled in Table S1. The plots are parallel lines and either at atmospheric pressure or at 30 bar the variations of E_a are insignificant: 33.2 ± 2.2 kJ.mol^{-1} vs. 34.3 ± 4.2 kJ.mol^{-1}, respectively. Therefore, the reaction mechanism does not change with pressure and is not affected by the preparation method, except perhaps for the cobalt–cerium catalyst obtained by *Pechini* method. Moreover, the values of the specific reaction rate constants for the formation of methane (k_{CH_4}, at 300 °C) were calculated to be 5682 ± 1410 mL/g.h and 7229 ± 1697 mL/g.h at atmospheric pressure and 30 bar, respectively. Considering the error, these values are very similar regardless of the pressure imposed on the system. That is to say that the pressure effect cannot be regarded as a pure kinetic effect that in general follows the *Langmuir–Hinshelwood–Hougen–Watson* model and the contribution of *Le Chatelier*'s principle (thermodynamics) also seems important. This agrees with the conclusions of other authors that have shown that higher pressures and low temperatures favor the methanation reaction accordingly to such principles [49].

3. Materials and Methods

3.1. Synthesis and Characterization

Nickel–cerium and cobalt–cerium bimetallic oxides were prepared by three different approaches and obtained as either nanoparticles or nanofibers and characterized as described by our group elsewhere [31]. For the Epoxide addition method, 4.5 mmol of $NiCl_2.6H_2O$ or $CoCl_2.6H_2O$ (Alfa Aesar; purity > 99.9%) and 1.5 mmol of $CeCl_3.7H_2O$ (Aldrich; purity > 99.9%) were dissolved in 6.3 mL of absolute ethanol in a flask. Subsequently, 3.8 mL of propylene oxide was added to the solution and the mixture was stirred for 5 min. The gel obtained was sealed in the preparation vessel and aged in absolute ethanol for 48 h at 50 °C, then dried by the organic solvent sublimation drying method (OSSD) using successive replacement solutions of 50%, 80%, and 100% of acetonitrile/ethanol (v/v), each one over 24 h at the same temperature of the aging stage. The aerogels were calcined at 500 °C under a heating rate of 1° C/min for 2 h. The product was ground and the grain size reduced to 200 mesh (75 μm). Using the *Pechini* method, 3.75 mmol of $Ni(NO_3)_2.6H_2O$ or $Co(NO_3)_2.6H_2O$ and 1.25 mmol of $Ce(NO_3)_3.6H_2O$ (Aldrich; purity > 99.9%) were mixed with 1.9 g of citric acid and 0.56 mL of ethylene glycol in 6.5 mL of deionized water (molar ratio, TMM: citric acid: ethylene glycol = 1:2:2; TMM is the total number of moles of metal nitrates in solution). The mixture was stirred until it formed a homogenous solution and then heated at 80–90 °C while stirring until the solution became a porous, wet gel. After that, the gel formed was dried for 5 h at 220 °C and then calcined at 500 °C for 2 h at a heating rate of a 1 °C/min. The final product was ground and sifted with a mesh of 75 μm. For catalysts prepared by Electrospinning technique, the metal salts, $Ni(NO_3)_2.6H_2O$ or $Co(NO_3)_2.6H_2O$ and $Ce(NO_3)_3.6H_2O$ (Aldrich, purity > 99.9%),) were dissolved in an appropriate stoichiometry (molar ratio of Ni or Co:Ce = 3) on the solution of 42 wt.% of polyvinylpyrrolidone (PVP) in absolute ethanol. For the Electrospinning experiments, the solution was collected in a syringe with a ~0.9 mm interior diameter stainless steel flat-tip needle, which was pumped continuously using a syringe pump (KW scientific) at a rate of 1 mL.h^{-1}, with an electric field of 15 kV applied between the syringe tip needle and a grounded aluminum plate placed 10 cm from the needle tip and used as a collector. The electrospun materials were subsequently calcined at 500 °C for 2h in air atmosphere at 1 °C.min^{-1}.

In this study, the samples were characterized after a reaction by XRD (X-ray powder diffraction), O_2-TPO (temperature-programmed oxidation), and H_2-TPR (temperature-programmed reduction). The diffraction patterns were obtained on a Bruker D2 PHASER diffractometer (Cu, kα monochromatic radiation, λ = 1.5406 Å, operational settings: voltage = 30 kV; current = 10 mA; 2θ scan range 20–80° using a step size of 0.03° and a time per step of 2 s), aiming to analyze the pressure effect on their crystalline structure (compared with standard JCPDS powder diffraction files [53]) and particle size (using the Scherrer equation). The O_2-TPO experiments were conducted in a commercial Micromeritics ChemiSorb 2720 unit equipped with the optional ChemiSoft TPx system using 10–20 mg of each used catalyst, a specific Micromeritics U-type quartz reactor, and a gaseous mixture of 10% O_2 in helium (flow rate of 20 mL.min^{-1}) at a heating rate of 10 °C/min from room temperature to 1050 °C. Moreover, considering the reactions that may occur, a qualitative and quantitative analysis of each O_2-TPO profile was performed. The qualitative analysis was performed by understanding the different oxidation steps. The quantitative analysis was performed through the total and partial O_2 consumption associated with each peak to quantify the oxidation of the metallic active phase (Ni, Co) and the amount of carbon present at the catalysts' surfaces after reaction. The O_2 uptakes were evaluated by integration of the experimental O_2-TPO curves, based on calibration measurements with Ni and Co generated in situ by the total reduction of commercial NiO and CuO powders (Aldrich, 99.99995% purity) (e.g., $Ni + 1/2O_2 \rightarrow NiO$; O_2 − uptake (mol) = $3.52 \times 10^{-5} \times$ Peak area). The H_2-TPR experiments were conducted in the same commercial Micromeritics ChemiSorb 2720 unit equipped with the optional ChemiSoft TPx system, also using 10−20 mg of each catalyst, a specific Micromeritics U-type quartz reactor, and a gaseous mixture of 10% H_2 in argon

(flow rate of 20 mL.min^{-1}) at a heating rate of 10 °C.min^{-1} from room temperature to 1050 °C. A qualitative and quantitative analysis of each H_2-TPR profile was also performed. The qualitative analysis was performed by understanding the different reduction steps and identifying and linking the maximum reduction temperature rates (T_m) of the different peaks to them. The quantitative analysis was performed by calculating the total and partial H_2 consumption associated with each step. The H_2 uptakes were evaluated by integration of the experimental H_2-TPR curves, based on calibration measurements with NiO powder (Aldrich, 99.99995% purity) ($NiO + H_2 \rightarrow Ni + H_2O$, H_2 − uptakes (mol) = $4.913 \times 10^{-6} \times$ Peak area).

3.2. Catalytic Studies

The CO_2 methanation studies were carried out in a stainless-steel (316 s) plug-flow-type reactor (quartz wool bed) at 300 °C and under pressures of 1, 10, 20, and 30 bar; reactor length 20 cm, reactor internal volume 15 cm^3. The catalysts' grain size was controlled using a 200 mesh sieve (0.074 mm). The amount of catalyst (m = 10–20 mg; max. 2 mm bed thickness, not diluted) was selected in such a way that rate limitation by external mass and heat transport processes under differential conditions were negligible by applying suitable experimental criteria, such as those defined by Mears (-rσRn/kC << 0.15) [54], Froment and Bischoff ($\Delta PCH_4 << 1 \times 10^{-4}$ atm; (DT) max << 1 K) [55], or Weiz and Prater (R^{2}r/CsDe << 0.3) [54]. A gaseous mixture of CO_2/H_2 (1:4 mol/mol) was used, and the reaction was studied with an adequate Gas Hourly Space Velocity (GHSV: 15,000 mL of CO_2 per g of catalyst and per h). Mass flow controllers (Bronkhorst) were used to control CO_2, H_2, and He flows, whereas pressure was controlled by a Bronkhorst EL-PRESS controller. Blank tests were also performed either at atmospheric pressure or under pressure (1–30 bar) and the only product observed was CO for a maximum CO_2 conversion of 1% at 500 °C/30 bar pressure.

The reactor outlet gas composition was analyzed online by gas chromatography using a Shimadzu 9A equipped with two detectors: a thermal conductivity detector (TCD) for the detection of all gaseous reagents and products, and a flame ionization detector (FID) for the detection of all condensable organic products, the first using a Restek ShinCarbon ST column (L = 2.0 m, 1/8 in., ID = 1mm, 100/200 mesh) and the second a Supelco 10% SP-2100 column (L = 1.8 m, 1/8 in., ID = 1mm, 100/200 mesh). The GC system is equipped with two pneumatic six-port gas-sampling valves (0.250 mL loops) for online TCD and FID analysis. Before TCD analysis, the outlet gas was cooled in an ice-water trap in order to avoid any column contamination, namely by water. Unless stated otherwise, all pure gases and mixtures were purchased from Air Liquide and supplied with an ALPHAGAZ 2 purity. The values reported in this paper represent the steady state activities after 1 h on stream at each pressure.

The catalysts' activity was defined as the volume of CH_4 converted per g of catalyst per hour (mL$_{CH4}$ g^{-1} h^{-1}). The conversion of CO_2 and selectivity to CH_4 and CO were calculated as follows: Conv. CO_2 (%) = ([CH_4]$_o$ + [CO]$_o$)/([CO]$_o$ + [CH_4]$_o$ + [CO_2]$_i$)×100; Sel. CH_4 (%) = [CH_4]$_o$/([CO]$_o$ + [CH_4]$_o$)×100; Sel.CO (%) = [CO]$_o$/([CO]$_o$ + [CH_4]$_o$)×100, where [CO_2]$_i$ is the inlet flow rate of CO_2 and [CO_2]$_o$, and [CH_4]$_o$ and [CO]$_o$ are the outlet flow rates of CO_2, CH_4, and CO. The calibration of the detectors was performed using external reference mixtures containing all reagents (H_2 and CO_2) and all expected products (CH_4, CO, C_2H_2, C_2H_4, C_2H_6, and C_3H_8). The confidence level was better than 95%.

The experimental procedure comprises the following steps: (i) pressure raise until 30 bar at indoor temperature (20 °C) using the reactional gaseous mixture; (ii) temperature increase until 300 °C; (iii) at that temperature, measure the catalytic activity at steady state (1 h reaction) at 30 bar and for each of the other pressures studied (20, 10, and 1 bar, atmospheric pressure) after controlled reactor depressurization and 1 h at steady state. All catalysts were tested after a pre-reduction treatment under hydrogen (10% H_2 in He) at 450 °C (30 min) using a 10 °C heating rate.

For comparison purposes, a commercial rhodium catalyst supported on alumina (Aldrich, $5_{wt.\%}$) was tested in the same experimental conditions. In all cases, the only products observed were methane, carbon monoxide, and minor quantities of C_2 hydrocarbons (selectivity $< 1\%$).

4. Conclusions

Nickel– and cobalt–cerium bimetallic oxides were very active and selective for the methanation of CO_2 and their activity and selectivity towards methane increases significantly under pressure. This effect is relevant for the nickel-based catalysts but very important in the case of the cobalt-based catalysts where the yield to methane increases from almost zero at atmospheric pressure to $50-60\%$ at 30 bar, whereas the selectivity increases from $40-60$ to $60-80\%$. Their performance also depends on the preparation method and the best results were those obtained over the catalysts prepared by the Electrospinning technique (fibers). Nickel– and cobalt–cerium bimetallic oxides are also remarkably competitive when compared to a rhodium catalyst used as a reference ($5_{wt.\%}$ Rh/Al_2O_3) and tested in the same conditions. The behavior of these catalysts can be mainly attributed to the formation of metallic Ni and Co phases. However, in the case of cobalt, the best results were those obtained over reused catalysts were Co and CoO synergistically coexist and to whom such good behavior was credited. We have also shown that the effect of pressure cannot be regarded as a pure kinetic effect that follows the *Langmuir–Hinshelwood–Hougen–Watson* model; the contribution of *Le Chatelier*'s principle is also important in order to explain the catalysts' behavior. Moreover, in the case of the cobalt–cerium bimetallic oxides, the formation of cobalt carbides may also play an important role on its catalytic behavior. Nevertheless, further work is needed in order to fully understand the cobalt-based catalysts' catalytic behavior, namely the synergetic effect between cobalt oxide and cobalt metallic phases and the importance of the formation of cobalt carbides.

Author Contributions: Conceptualization, J.M.B.B. and A.C.F.; data curation, J.F.M.; formal analysis, J.M.B.B. and A.C.F.; funding acquisition, A.C.F.; investigation, J.M.B.B., J.F.M. and A.C.F.; methodology, J.M.B.B. and A.C.F.; project administration, A.C.F.; resources, J.M.B.B.; supervision, J.M.B.B.; writing—original draft, J.M.B.B.; writing—review and editing, J.M.B.B. and A.C.F. All authors have read and agreed to the published version of the manuscript.

Data Availability Statement: Not applicable.

References

1. Ashok, J.; Pati, S.; Hongmanorom, P.; Tianxi, Z.; Junmei, C.; Kawi, S. A review of recent catalyst advances in CO_2 methanation processes. *Catal. Today* **2020**, *356*, 471–489. [CrossRef]
2. Thema, M.; Bauer, F.; Sterner, M. Power-to-Gas: Electrolysis and methanation status review. *Renew. Sustain. Energ. Rev.* **2019**, *112*, 775–787. [CrossRef]
3. Gotz, M.; Lefebvre, J.; Mors, F.; Koch, A.M.; Graf, F.; Bajohr, S.; Reimert, R.; Kolb, T. Renewable Power-to-Gas: A technological and economic review. *Renew. Energ.* **2016**, *85*, 1371–1390. [CrossRef]
4. Melaet, G.; Ralston, W.T.; Li, C.S.; Alayoglu, S.; An, K.; Musselwhite, N.; Kalkan, B.; Somorjai, G.A. Evidence of Highly Active Cobalt Oxide Catalyst for the Fischer-Tropsch Synthesis and CO_2 Hydrogenation. *J. Am. Chem. Soc.* **2014**, *136*, 2260–2263. [CrossRef]
5. Pan, Q.S.; Peng, J.X.; Sun, T.J.; Wang, S.; Wang, S.D. Insight into the reaction route of CO_2 methanation: Promotion effect of medium basic sites. *Catal. Commun.* **2014**, *45*, 74–78. [CrossRef]
6. Dauenhauer, P.J.; Dreyer, B.J.; Degenstein, N.J.; Schmidt, L.D. Millisecond reforming of solid biomass for sustainable fuels. *Angew. Chem. Int. Edit.* **2007**, *46*, 5864–5867. [CrossRef]
7. Bacariza, M.C.; Spataru, D.; Karam, L.; Lopes, J.M.; Henriques, C. Promising Catalytic Systems for CO_2 Hydrogenation into CH_4: A Review of Recent Studies. *Processes* **2020**, *8*, 1646. [CrossRef]
8. Sreedhar, I.; Varun, Y.; Singh, S.A.; Venugopal, A.; Reddy, B.M. Developmental trends in CO_2 methanation using various catalysts. *Catal. Sci. Technol.* **2019**, *9*, 4478–4504. [CrossRef]
9. Janlamool, J.; Praserthdam, P.; Jongsomjit, B. Ti-Si composite oxide-supported cobalt catalysts for CO_2 hydrogenation. *J. Nat. Gas Chem.* **2011**, *20*, 558–564. [CrossRef]
10. Branco, J.B.; da Silva, R.P.; Ferreira, A.C. Methanation of CO_2 over Cobalt-Lanthanide Aerogels: Effect of Calcination Temperature. *Catalysts* **2020**, *10*, 704. [CrossRef]
11. Kwak, J.H.; Kovarik, L.; Szanyi, J. CO_2 Reduction on Supported Ru/Al_2O_3 Catalysts: Cluster Size Dependence of Product Selectivity. *ACS Catal.* **2013**, *3*, 2449–2455. [CrossRef]
12. Beuls, A.; Swalus, C.; Jacquemin, M.; Heyen, G.; Karelovic, A.; Ruiz, P. Methanation of CO_2: Further insight into the mechanism over $Rh/gamma-Al_2O_3$ catalyst. *Appl. Catal. B-Environ.* **2012**, *113*, 2–10. [CrossRef]
13. Kwak, J.H.; Kovarik, L.; Szanyi, J. Heterogeneous Catalysis on Atomically Dispersed Supported Metals: CO_2 Reduction on Multifunctional Pd Catalysts. *ACS Catal.* **2013**, *3*, 2094–2100. [CrossRef]
14. Ocampo, F.; Louis, B.; Kiwi-Minsker, L.; Roger, A.C. Effect of Ce/Zr composition and noble metal promotion on nickel based $Ce_xZr_{1-x}O_2$ catalysts for carbon dioxide methanation. *Appl. Catal. A-Gen.* **2011**, *392*, 36–44. [CrossRef]
15. Massa, F.; Coppola, A.; Scala, F. A thermodynamic study of sorption-enhanced CO_2 methanation at low pressure. *J. CO2 Util.* **2020**, *35*, 176–184. [CrossRef]
16. Gao, J.J.; Wang, Y.L.; Ping, Y.; Hu, D.C.; Xu, G.W.; Gu, F.N.; Su, F.B. A thermodynamic analysis of methanation reactions of carbon oxides for the production of synthetic natural gas. *RSC Adv.* **2012**, *2*, 2358–2368. [CrossRef]
17. Skrzypek, J.; Lachowska, M.; Grzesik, M.; Sloczynski, J.; Nowak, P. Thermodynamics and Kinetics of Low-Pressure Methanol Synthesis. *Chem. Eng. J. Biochem. Eng.* **1995**, *58*, 101–108. [CrossRef]
18. Gaikwad, R.; Bansode, A.; Urakawa, A. High-pressure advantages in stoichiometric hydrogenation of carbon dioxide to methanol. *J. Catal.* **2016**, *343*, 127–132. [CrossRef]
19. Hansen, J.B.; Højlund Nielsen, P.E. Methanol Synthesis. In *Handbook of Heterogeneous Catalysis*; Wiley-VCH Verlag GmbH & Co. KGaA: Weinheim, Germany, 2008.
20. BASF, German Patent n° 415 686, 441 433 and 462 837, 1923. Available online: https://patents.google.com/patent/WO2017140800A1/en (accessed on 27 December 2021).
21. Bahmanpour, A.M.; Signorile, M.; Krocher, O. Recent progress in syngas production via catalytic CO_2 hydrogenation reaction. *Appl. Catal. B-Environ.* **2021**, *295*, 120319. [CrossRef]
22. Ciesielski, R.; Shtyka, O.; Zakrzewski, M.; Kubicki, J.; Maniukiewicz, W.; Kedziora, A.; Maniecki, T.P. Mechanistic Studies of Methanol Synthesis Reaction over Cu and Pd-Cu Catalysts. *Kinet. Catal.* **2020**, *61*, 623–630. [CrossRef]
23. Ipatieff, V.N.; Monroe, G.S. Synthesis of Methanol from Carbon Dioxide and Hydrogen over Copper Alumina Catalysts— Mechanism of Reaction. *J. Am. Chem. Soc.* **1945**, *67*, 2168–2171. [CrossRef]
24. Luna, M.L.; Timoshenko, J.; Kordus, D.; Rettenmaier, C.; Chee, S.W.; Hoffman, A.S.; Bare, S.R.; Shaikhutdinov, S.; Cuenya, B.R. Role of the Oxide Support on the Structural and Chemical Evolution of Fe Catalysts during the Hydrogenation of CO_2. *ACS Catal.* **2021**, *11*, 6175–6185. [CrossRef]
25. Franken, T.; Heel, A. Are Fe based catalysts an upcoming alternative to Ni in CO_2 methanation at elevated pressure? *J. CO2 Util.* **2020**, *39*, 101175. [CrossRef]
26. Li, W.H.; Liu, Y.; Mu, M.C.; Ding, F.S.; Liu, Z.M.; Guo, X.W.; Song, C.S. Organic acid-assisted preparation of highly dispersed Co/ZrO_2 catalysts with superior activity for CO_2 methanation. *Appl. Catal. B-Environ.* **2019**, *254*, 531–540. [CrossRef]
27. Zhou, Y.W.; Jiang, Y.X.; Qin, Z.Z.; Xie, Q.R.; Ji, H.B. Influence of Zr, Ce, and La on Co_3O_4 catalyst for CO_2 methanation at low temperature. *Chin. J. Chem. Eng.* **2018**, *26*, 768–774. [CrossRef]
28. Jimenez, J.D.; Wen, C.; Lauterbach, J. Design of highly active cobalt catalysts for CO_2 hydrogenation via the tailoring of surface orientation of nanostructures. *Catal. Sci. Technol.* **2019**, *9*, 1970–1978. [CrossRef]

29. Li, W.H.; Nie, X.W.; Jiang, X.; Zhang, A.F.; Ding, F.S.; Liu, M.; Liu, Z.M.; Guo, X.W.; Song, C.S. ZrO_2 support imparts superior activity and stability of Co catalysts for CO_2 methanation. *Appl. Catal. B-Environ.* **2018**, *220*, 397–408. [CrossRef]

30. Jampaiah, D.; Damma, D.; Chalkidis, A.; Venkataswamy, P.; Bhargava, S.K.; Reddy, B.M. MOF-derived ceria-zirconia supported Co_3O_4 catalysts with enhanced activity in CO_2 methanation. *Catal. Today* **2020**, *356*, 519–526. [CrossRef]

31. Branco, J.B.; Ferreira, A.C.; Vieira, F.; Martinho, J.F. Cerium-Based Bimetallic Oxides as Catalysts for the Methanation of CO_2: Influence of the Preparation Method. *Energy Fuels* **2021**, *35*, 6725–6737. [CrossRef]

32. Branco, J.B.; Ferreira, A.C.; Goncalves, A.P.; Soares, C.O.; Gasche, T.A. Synthesis of methanol using copper-*f* block element bimetallic oxides as catalysts and greenhouse gases (CO_2, CH_4) as feedstock. *J. Catal.* **2016**, *341*, 24–32. [CrossRef]

33. Li, Z.H.; Si, M.Y.; Xin, L.; Liu, R.J.; Liu, R.X.; Lu, J. Cobalt catalysts for Fischer-Tropsch synthesis: The effect of support, precipitant and pH value. *Chin. J. Chem. Eng.* **2018**, *26*, 747–752. [CrossRef]

34. Zhao, K.; Calizzi, M.; Moioli, E.; Li, M.; Borsay, A.; Lombardo, L.; Mutschler, R.; Luo, W.; Zuttel, A. Unraveling and optimizing the metal-metal oxide synergistic effect in a highly active Co_xCoO_{1-x} catalyst for CO_2 hydrogenation. *J. Energy Chem.* **2021**, *53*, 241–250. [CrossRef]

35. Puga, A.V. On the nature of active phases and sites in CO and CO_2 hydrogenation catalysts. *Catal. Sci. Technol.* **2018**, *8*, 5681–5707. [CrossRef]

36. Manukyan, K.V.; Avetisyan, A.G.; Shuck, C.E.; Chatilyan, H.A.; Rouvimov, S.; Kharatyan, S.L.; Mukasyan, A.S. Nickel Oxide Reduction by Hydrogen: Kinetics and Structural Transformations. *J. Phys. Chem. C* **2015**, *119*, 16131–16138. [CrossRef]

37. Tomic-Tucakovic, B.; Majstorovic, D.; Jelic, D.; Mentus, S. Thermogravimetric study of the kinetics of Co_3O_4 reduction by hydrogen. *Thermochim. Acta* **2012**, *541*, 15–24. [CrossRef]

38. Lin, Q.; Liu, B.; Jiang, F.; Fang, X.J.; Xu, Y.B.; Liu, X.H. Assessing the formation of cobalt carbide and its catalytic performance under realistic reaction conditions and tuning product selectivity in a cobalt-based FTS reaction. *Catal. Sci. Technol.* **2019**, *9*, 3238–3258. [CrossRef]

39. Alotaibi, N.; Hammud, H.H.; Karnati, R.K.; Hussain, S.G.; Mazher, J.; Prakasam, T. Cobalt-carbon/silica nanocomposites prepared by pyrolysis of a cobalt 2,2′-bipyridine terephthalate complex for remediation of cationic dyes. *RSC Adv.* **2020**, *10*, 17660–17672. [CrossRef]

40. Kwak, G.; Kim, D.E.; Kim, Y.T.; Park, H.G.; Kang, S.C.; Ha, K.S.; Jun, K.W.; Lee, Y.J. Enhanced catalytic activity of cobalt catalysts for Fischer-Tropsch synthesis via carburization and hydrogenation and its application to regeneration. *Catal. Sci. Technol.* **2016**, *6*, 4594–4600. [CrossRef]

41. Choi, Y.I.; Yang, J.H.; Park, S.J.; Sohn, Y. Energy Storage and CO_2 Reduction Performances of $Co/Co_2C/C$ Prepared by an Anaerobic Ethanol Oxidation Reaction Using Sacrificial SnO_2. *Catalysts* **2020**, *10*, 1116. [CrossRef]

42. Dai, E.G.; Xu, J.; Qiu, J.J.; Liu, S.C.; Chen, P.; Liu, Y. Co@Carbon and Co_3O_4@Carbon nanocomposites derived from a single MOF for supercapacitors. *Sci. Rep.* **2017**, *7*, 12588. [CrossRef] [PubMed]

43. Kim, J.H.; Kawashima, K.; Wygant, B.R.; Mabayoje, O.; Liu, Y.; Wang, J.H.; Mullins, C.B. Transformation of a Cobalt Carbide (Co_3C) Oxygen Evolution Precatalyst. *Acs Appl Energ. Mater* **2018**, *1*, 5145–5150. [CrossRef]

44. Kim, M.; Nam, D.H.; Park, H.Y.; Kwon, C.; Eom, K.; Yoo, S.; Jang, J.; Kim, H.J.; Cho, E.; Kwon, H. Cobalt-carbon nanofibers as an efficient support-free catalyst for oxygen reduction reaction with a systematic study of active site formation. *J. Mater Chem. A* **2015**, *3*, 14284–14290. [CrossRef]

45. Schild, C.; Wokaun, A.; Baiker, A. On the Mechanism of CO and CO_2 Hydrogenation Reactions on Zirconia-Supported Catalysts— A Diffuse Reflectance FTIR Study.1. Identification of Surface Species and Methanation Reactions on Palladium Zirconia Catalysts. *J. Mol. Catal.* **1990**, *63*, 223–242. [CrossRef]

46. Bui, M.; Adjiman, C.S.; Bardow, A.; Anthony, E.J.; Boston, A.; Brown, S.; Fennell, P.S.; Fuss, S.; Galindo, A.; Hackett, L.A.; et al. Carbon capture and storage (CCS): The way forward. *Energ. Environ. Sci.* **2018**, *11*, 1062–1176. [CrossRef]

47. Lapidus, A.L.; Gaidai, N.A.; Nekrasov, N.V.; Tishkova, L.A.; Agafonov, Y.A.; Myshenkova, T.N. The mechanism of carbon dioxide hydrogenation on copper and nickel catalysts. *Pet. Chem.* **2007**, *47*, 75–82. [CrossRef]

48. Miguel, V.; Mendes, A.; Madeira, L.M. Intrinsic kinetics of CO_2 methanation over an industrial nickel-based catalyst. *J. CO2 Util.* **2018**, *25*, 128–136. [CrossRef]

49. Koytsoumpa, E.I.; Karellas, S. Equilibrium and kinetic aspects for catalytic methanation focusing on CO_2 derived Substitute Natural Gas (SNG). *Renew. Sustain. Energ. Rev.* **2018**, *94*, 536–550. [CrossRef]

50. Dew, J.N.; White, R.R.; Sliepcevich, C.M. Hydrogenation of Carbon Dioxide on Nickel-Kieselguhr Catalyst. *Ind. Eng. Chem.* **1955**, *47*, 140–146. [CrossRef]

51. Chiang, J.H.; Hopper, J.R. Kinetics of the Hydrogenation of Carbon-Dioxide over Supported Nickel. *Ind. Eng. Chem. Prod. Res. Dev.* **1983**, *22*, 225–228. [CrossRef]

52. Herwijnen, T.V.; Doesburg, H.V.; Dejong, W.A. Kinetics of Methanation of CO and CO_2 on a Nickel-Catalyst. *J. Catal.* **1973**, *28*, 391–402. [CrossRef]

53. JCPDS. *The Powder Diffraction File*; JCPDS: Swarthmore, PA, USA, 1981.

54. Oyama, S.T.; Zhang, X.M.; Lu, J.Q.; Gu, Y.F.; Fujitani, T. Epoxidation of propylene with H_2 and O_2 in the explosive regime in a packed-bed catalytic membrane reactor. *J. Catal.* **2008**, *257*, 1–4. [CrossRef]

55. Froment, G.F.; Bischoff, K.B. *Chemical reactor Anaylsis and Design*; John Wiley & Sons: Hoboken, NJ, USA, 1979.